Self-Assembly and Crystallization in a Supramolecular Hairy Rod Polymer from the Complex of Polyaniline with ω-Methoxy Poly(ethylene oxide) Phosphates

Bhanu Nandan,[†] Hsin-Lung Chen,*[,†] Chien-Shiun Liao,[‡] and Show-An Chen[†]

Department of Chemical Engineering, National Tsing Hua University, Hsin-Chu, Taiwan 30013, R.O.C., and Department of Chemical Engineering and Material Science, Yuan Ze University, Nei-Li, Taoyuan, Taiwan 320, R.O.C

Received August 5, 2004; Revised Manuscript Received September 22, 2004

ABSTRACT: A semirigid conjugated polyaniline (PANI) was complexed with a ω-methoxy poly(ethylene oxide) phosphate (PEOPA) through ionic bonding to yield a supramolecular hairy rod polymer comprised of an ionic PANI backbone and nonionic PEO side chains. The strong backbone−side chain repulsion resulted in a microphase-separated lamellar morphology consisting of alternating ionic and nonionic layers irrespective of the binding fraction. The thickness of the PEO layer increased with increasing binding fraction due to the smaller interfacial area per PEO chain at higher binding fraction which resulted in its higher stretching normal to the lamellar interface. The complex exhibited an order−disorder transition near 225 °C driven by deprotonation. The conformational rigidity of PANI backbone coupled with the strong backbone−side chain bonding strongly retarded the crystallization kinetics and the crystallizability of the PEO side chains in the complexes.

Introduction

The process of self-organization facilitates formation of ordered polymer nanostructures. It is well-known that block copolymers self-organize into a series of long-range ordered nanostructures due to repulsion between the covalently connected blocks.[1−3] Similar to block copolymers are polymers with comb-shaped architecture which also exhibit a tendency to self-organize in essentially similar way.[4] A special case consists of the so-called "hairy rod polymers" where there are flexible side chains covalently bonded to rigid or semirigid backbones.[5−8] Here, the comb-shaped architecture is of special importance as it also induces fusibility and solubility in a straightforward way to the otherwise intractable backbone.

In comb-shaped polymers, the covalent or permanent bonding between the backbone and the repulsive side chains may be replaced by weaker interactions such as ionic bonds, hydrogen bonds, and metal-mediated coordination bonds to form supramolecules which may analogically self-organize to form mesomorphic nanostructures.[9−19] Application of this concept to rodlike conjugated polymers to generate "supramolecular hairy rod polymers" would be of interest since it could lead to new optoelectronic materials through a simple preparative approach.[17,18,20,21]

Polyaniline (PANI) is one of the most promising conjugated conducting polymers due to its straightforward polymerization and excellent chemical stability combined with relatively high levels of conductivity. The so-called emeraldine base (EB) form of PANI **(I)** is half-oxidized and thus consists of phenylenediamine and quinoid diimine units. Emeraldine base is insulating, but its iminic nitrogen sites can be protonated by strong acids to form an acid−base complex which is conducting. This electrically conductive form is called emeraldine salt **(II)**. A fully protonated conductive complex is formed when 1 mol of PhN unit in PANI is reacted with ca. 0.5 mol of protonic acid. Usually functional organic acid such as camphorsulfonic acid (CSA) or dodecylbenzenesulfonic acid (DBSA) has been used as a dopant. Polyaniline doped through these functional organic acids can only be processed through some organic solvents. As far as environmental issues are concerned, processing from aqueous systems is important. Recently, a water-soluble conducting PANI has been prepared by ionic complexation with a phosphoric acid-terminated poly(ethylene oxide) (PEO), i.e., ω-methoxy poly(ethylene oxide) phosphates (PEOPA). The acid headgroup of PEOPA acts as the protonic acid dopant for PANI while the long hydrophilic PEO tails render the complex water-soluble.[22,23]

Apart from the advantage of water solubility, PANI(PEOPA) complexes also represent a supramolecular hairy rod polymer which may exhibit a tendency toward self-organization. In this case, the repulsion between the dissimilar PANI rigid backbone and flexible PEO side chains will drive the complex toward a macrophase separation whereas the attraction between them because of the ionic bonding will oppose it ultimately leading to microphase separation in the system.

In the present article we investigate the self-assembled structure of PANI(PEOPA) complexes. In contrast to the previously studied supramolecular comb polymers comprising predominantly of polymer−surfactant complexes in which the polymer backbone and the surfactant alkyl chains have widely different polarity, both the PANI backbone and the PEO side chains in the present system are polar. Nevertheless, it will be demonstrated that a microphase separation between these two units is still accessible in the complex due to their low entropy of mixing. The effect of binding fraction on the self-assembled structure of the complexes will also be examined here. Furthermore, the oligomeric PEO side chains in the hairy rod complexes exhibit a

[†] National Tsing Hua University.
[‡] Yuan Ze University.
* To whom correspondence should be addressed.

10.1021/ma048384r CCC: $27.50
Published on Web 11/16/2004

Scheme 1

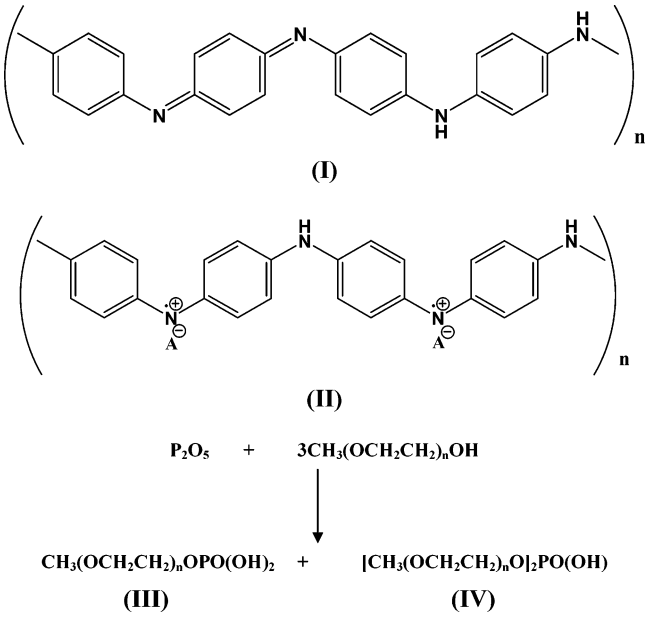

tendency to crystallize at subambient temperatures; therefore, the crystallization of PEO chains in the microdomains of the self-assembled complexes is also systematically investigated.

Experimental Section

Materials. PEOPA was synthesized from poly(ethylene glycol) monomethyl ether (PEGME) ($M_n = 550$) and phosphorus pentaoxide (P_2O_5) using a reported method shown in Scheme 1.[22] In a typical reaction, 0.3 mol of PEGME in 50 mL of benzene was added into a dispersion of 0.1 mol of P_2O_5 (14.16 g) in 50 mL of benzene. The mixture was heated to 70 °C and stirred for 3 h. After removing residual P_2O_5 and solvent, a colorless transparent liquid was obtained. As shown in Scheme 1, the product **(III** and **IV)** is a mixture of mono- and bihydroxyl acids with a molar ratio of 1:1. The average molecular weight of the PEOPA was estimated to be 896. PANI was synthesized by the oxidative polymerization of its monomers in 1 M aqueous HCl with $(NH_4)_2S_2O_8$ as oxidant followed by further reducing to EB form with dilute ammonium hydroxide solution according to literature procedures.[24]

Sample Preparation. PANI(PEOPA)$_R$ complexes were prepared from aqueous solution, where R denotes the binding fraction given by the average number of PEOPA molecules bound to one monomer unit of PANI. The PANI/PEOPA physical mixture in a suitable molar ratio was dissolved in freshly distilled water at a concentration of 20 mg/mL. The aqueous solution was subsequently magnetically stirred for 5 days at room temperature to obtain a clear solution. The formation of the PANI(PEOPA)$_R$ complex **(V)** is shown in Scheme 2. The conducting film of the the PANI(PEOPA)$_R$ complex was obtained from the preceding solution by casting it in a Petri dish and drying on a hot plate at 50 °C followed by further drying in vacuo at 40 °C for 24 h. The binding fractions of the complexes studied here and the corresponding PEOPA/PANI weight ratios are presented in Table 1.

UV−Vis Spectroscopy. An ultraviolet−visible spectrophotometer (UV−vis spectrometer, Jasco 310) was utilized to verify the complex formation. The spectra in the wavelength range of 200−1200 nm were recorded from the 1 mg/mL aqueous solutions of PANI(PEOPA)$_R$ complexes.

Differential Scanning Calorimetry. The nonisothermal crystallization study of the PEO side chains in PANI(PEOPA)$_R$ complexes was carried out using a TA Instrument 2000 differential scanning calorimeter (DSC) equipped with the RCS cooling system. Calibration for temperature and heat flow was made prior to sample analysis using indium as the standard.

Scheme 2

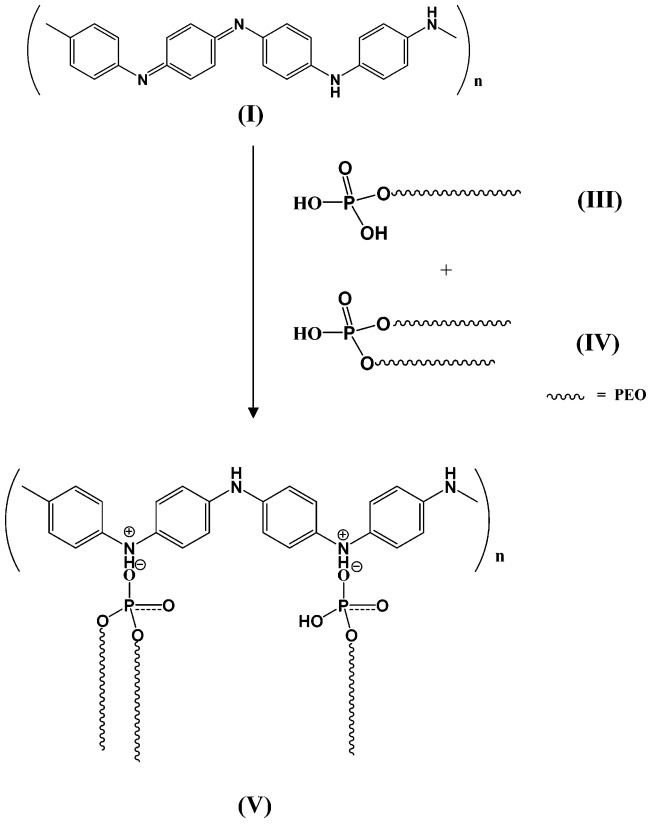

Table 1. Compositions of PANI(PEOPA)$_R$ Complexes Studied

binding fraction (R)	wt % ratio (PEOPA/PANI)	binding fraction (R)	wt % ratio (PEOPA/PANI)
1.0	90.8/9.2	0.3	74.7/25.3
0.7	87.3/12.7	0.2	66.3/33.7
0.5	83.1/16.9		

All measurements were carried out with the sample in a nitrogen atmosphere. Sample size was maintained around 3.5 mg. Each sample was first heated to 75 °C, which is well above the melting point of PEO, and then was kept at this temperature for 5 min to ensure complete melting of the crystals. The samples were then cooled at constant cooling rates (1, 2, 5, and 8 °C/min), and the exothermic crystallization peaks were recorded. The melting endotherms were subsequently recorded by heating the samples at a rate of 10 °C/min.

SAXS Measurements. SAXS measurements were performed using a Bruker NanoSTAR SAXS instrument. The X-ray source, a 1.5 kW X-ray generator (Kristalloflex 760) equipped with a Cu tube, was operated at 35 mA and 40 kV. The scattering intensity was detected by a two-dimensional position-sensitive detector (Bruker AXS) with 512 × 512 channels. The area scattering pattern has been radially averaged to increase the photon counting efficiency compared with the one-dimensional linear detector. The intensity profile was output as the plot of the scattering intensity (I) vs the scattering vector, $q = 4\pi/\lambda \sin(\theta/2)$ (θ = scattering angle). All data were corrected by the empty beam scattering, the sensitivity of each pixel of the area detector, and thermal diffuse scattering (I_{TDS}). The thermal diffuse scattering was considered as a positive deviation from the Porod law[25,26] and may be associated with thermal motion, local disorder, or frozen-in fluctuations. I_{TDS} can be regarded as a constant background, and the total scattered intensity in the high-q region is expressed by the Porod−Ruland equation[27]

$$I(q) = \frac{K_P \exp(-\sigma^2 q^2)}{q^4} + I_{TDS} \quad (1)$$

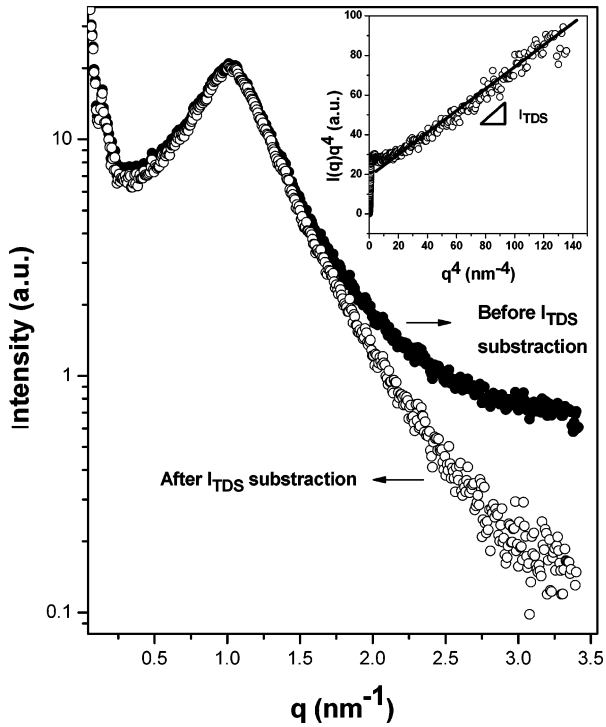

Figure 1. An illustration of the contribution from thermal diffuse scattering to the total scattered intensity in a typical SAXS profile. The inset demonstrates how I_{TDS} is determined from the slope of the $I(q)q^4$ vs q^4 plot.

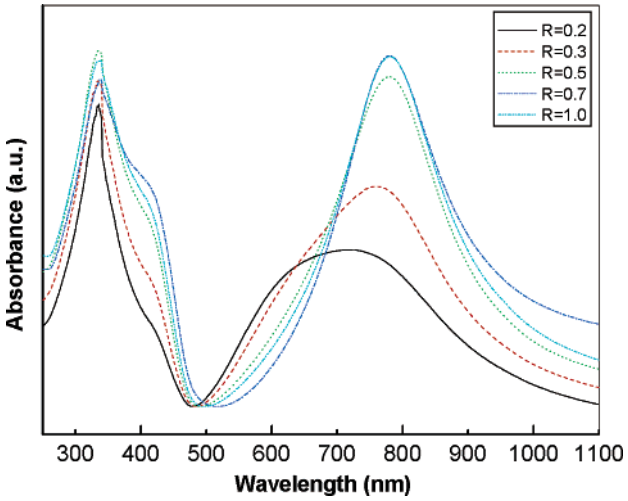

Figure 2. UV−vis absorption spectra of PANI(PEOPA)$_R$ complexes with different binding fractions measured in aqueous solution.

where K_P is the Porod's constant and σ is a parameter related to the thickness of interphase for a two-phase structure. The exponential term in eq 1 becomes insignificant at sufficiently high q such that a plot of $I(q)q^4$ vs q^4 would yield a straight line with a slope given by I_{TDS}, as demonstrated in the inset of Figure 1. The effect of I_{TDS} on the intensity profile in the high-q region is also demonstrated in Figure 1 showing the SAXS profile before and after I_{TDS} subtraction.

Results and Discussion

Complex Formation. First, UV−vis spectroscopy was performed to study the complex formation between PANI and PEOPA. Figure 2 shows the absorption spectra of PANI(PEOPA)$_R$ complexes in aqueous solution with different binding fractions. The commonly reported UV−vis spectrum of PANI has two absorption

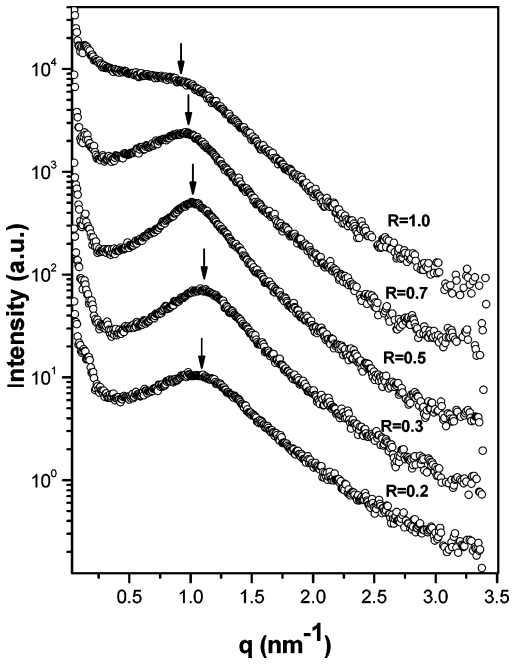

Figure 3. Representative room temperature SAXS profiles of PANI(PEOPA)$_R$ complexes. The binding fractions are indicated in the figure. The scattering peak associated with the microphase separation shifts to lower q with increasing binding fraction.

peaks near 300 and 600 nm, which has been attributed to the $\pi-\pi^*$ transition of the benzenoid rings and the exciton absorption of the quinoid rings, respectively.[28,29] The PANI structure in the emeraldine base form (**I**) has half of the nitrogen atoms in amine groups and the other half in imine groups. Since only the imine groups can be doped by protonic acids, the stoichiometric binding fraction is $R = 0.5$. While the nitrogen atoms in the imine groups are protonated, nitrogen and its neighboring quinoid ring become a semiquinoid radical cation, and the intensity of the exciton absorption peak near 600 nm decreases. Hence, the intensity of peak near 600 nm gives an idea about the extent of doping of PANI chains. As can be observed from Figure 2, the exciton absorption peak completely disappears for the stoichiometric ($R = 0.5$) and higher binding fractions, since all the imine groups are completely protonated at these compositions. At lower binding fractions of $R = 0.2$ and 0.3, the exciton peak still persists, which indicates incomplete doping of PANI chains. The doping of PANI chains can also be followed by the appearance of absorption peaks due to polaron band transitions at around 400 and 800 nm. As can be observed from Figure 2, two new peaks emerge near 400 and 800 nm with their intensities increasing with increasing binding fraction, which reveals a higher extent of doping at larger R. The decrease of the intensity of the polaron band transitions at 400 nm in the case of $R = 1.0$ may be caused by the increase in counteranion concentration that leads to the shielding of positive charges along the polymer backbone from one another.[30] This results in less repulsion between polaron's and hence allows the chains to coil slightly leading to a decrease in the conjugation length as well as polaron's delocalization length. Thus, the UV−vis data give enough evidence to suggest an efficient doping of PANI chains by PEOPA. Also, it must be mentioned that the PANI chains should adopt the highest planar conformation at $R = 0.5$, as at lower binding fraction doping is still not complete

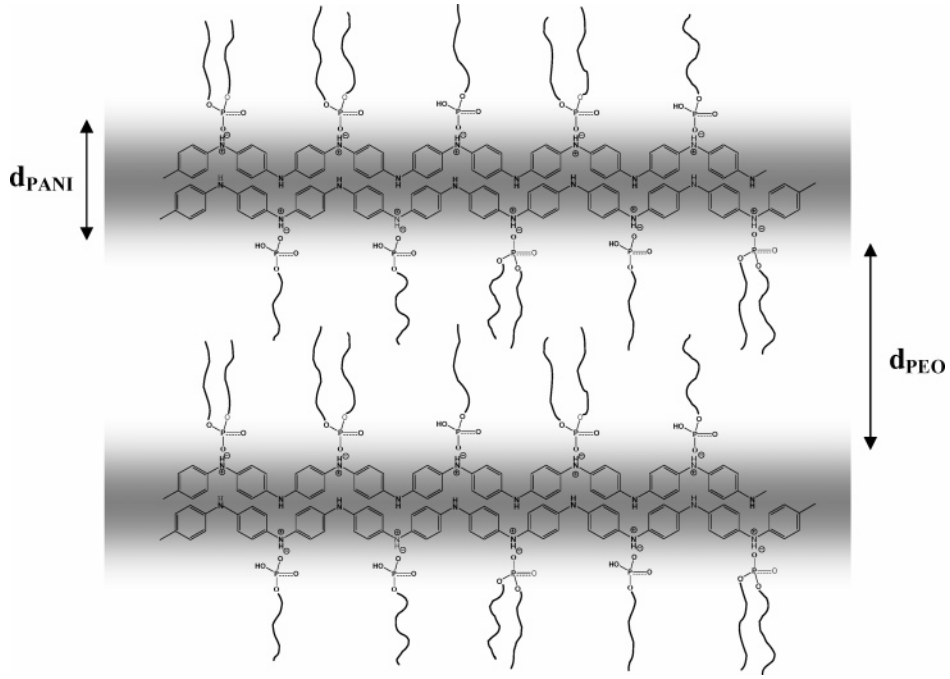

Figure 4. Schematic illustration of the proposed lamellar structure consisting of alternating ionic layer (including the protonated PANI chains and the phosphate groups of PEOPA) and nonionic layer (consisting of PEO chains). The PEO chains are supposed to be significantly stretched with a limited interdigitation in a direction perpendicular to the lamellar interface.

whereas at higher doping ratios the excess dopant tends to shield the repulsion between two polarons.

Microphase Separation and Self-Assembled Structure in the Bulk State. SAXS is employed to probe the supramolecular structure of PANI(PEOPA)$_R$ complexes in the bulk state. Figure 3 displays the SAXS profiles of these complexes at room temperature. It is noted that the PEO side chains have sufficiently low molecular weight to remain in melt state (i.e., uncrystalline) at room temperature, and hence the SAXS profiles observed are entirely due to the melt structure of the complexes. An intense maximum is observed in the scattering profiles of all complexes, signaling the formation of microphase-separated structure. Nevertheless, the absence of higher order peaks in the scattering profiles necessitates a closer evaluation of the SAXS data. It is well-known that comb-shaped polymers in the disordered state may exhibit characteristic block copolymer-like concentration fluctuations, which may also lead to a SAXS peak (i.e., the so-called "correlation hole" peak).[16] Such a correlation hole effect can be ruled out here considering that the peak observed in Figure 3 is sharper than the typical correlation hole peak. Moreover, the SAXS intensity due to contribution from concentration fluctuations usually follows the well-known Ornstein−Zernicke equation[31] which prescribes a q^{-2} dependence for the scattered intensity in the high-q region. In the present case, however, the slope of the log−log plots of $I(q)$ vs q at high q is about −4, which corresponds to the scattering from a two-phase system with sharp phase boundary given by the Porod's law.[25,26] This emphatically suggests that the peak observed in the SAXS profiles in Figure 3 arises from a microphase separation in PANI(PEOPA)$_R$ complexes.

Since the higher order peaks are absent, a detailed evaluation of the SAXS data is necessary for assigning the microphase-separated structure of the complexes. Considering that the lamellar phase has mostly been observed in comblike polymers with both flexible and rigid main chains, an assumption of a layered structure for the present system should be the most plausible. This assumption is reasonable also considering that the recent theoretical treatment of the phase behavior of supramolecular hairy rod polymers has predicted the lamellar phase to be the predominant structure while the other possible hexagonally packed cylinder structure would appear at relatively higher volume fraction of the rod.[20,21] Hence, the SAXS peaks observed in Figure 3 have been attributed to the lamellar morphology in the complexes. A schematic illustration of the proposed lamellar structure is shown in Figure 4. The lamellar phase consists of alternating layers of conjugated polymer including the ionic headgroups of PEOPA (thickness = d_{PANI}) and layers of PEO chains (thickness = d_{PEO}). The position of the SAXS peak (q_m) yields a measure of the interlamellar distance ($L = d_{PANI} + d_{PEO} = 2\pi/q_m$) via Bragg's law. The scattering peak is seen to shift to lower q with increase of binding fraction, showing a swelling of the interlamellar distance. The breadth of the SAXS peak also varies with binding fraction, indicating different degrees of lamellar organization in the complexes, where a broader peak signals a higher defect density in terms of the internal order and coherent length of lamellar stacking.[32]

For visualizing a complete picture of the lamellar morphology, the thicknesses of the individual layers, i.e., d_{PANI} and d_{PEO}, must be evaluated. These morphological parameters may be determined conveniently from the one-dimensional correlation function, $\gamma_1(z)$, defined as[33]

$$\gamma_1(z) = \frac{\int_0^\infty I(q) q^2 \cos(qz)\, dq}{\int_0^\infty I(q) q^2\, dq} \qquad (2)$$

Since the experimentally accessible q range is finite, extrapolation to both low and high q is necessary for the integration in eq 2. In the present work, extrapolation to zero q was accomplished by applying the Debye−Bueche model,[34,35] whereas the Porod−Ruland model[27] was used for extension to large q.

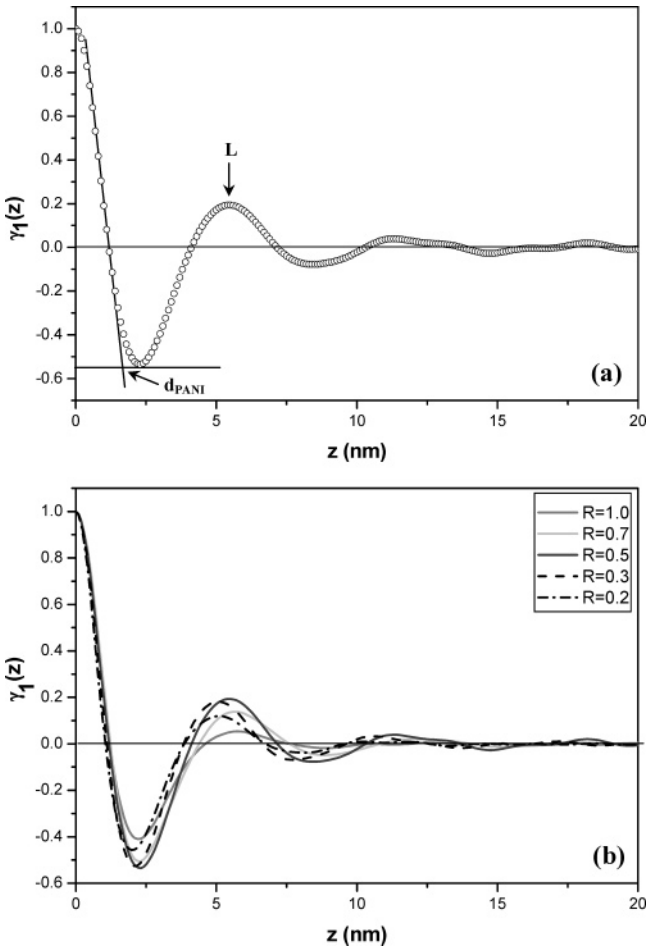

Figure 5. (a) A demonstration for the determinations of PANI layer thickness (d_{PANI}) and interlamellar distance (L) from the one-dimensional correlation function calculated from the SAXS profile. (b) One-dimensional correlation functions of PANI(PEOPA)$_R$ complexes with different binding fractions.

Figure 5a shows the typical one-dimensional correlation function plot of PANI(PEOPA)$_R$ complex with $R = 0.5$ for illustrating the determination of the layer thickness. The first maximum yields the most probable value of the interlamellar distance.[33,36] Intersection of the baseline with the straight line extended from the self-correlation triangle yields the average thickness of the thinner layer in the lamellar stacks, which is d_{PANI} in this case. Figure 5b displays the $\gamma_1(z)$s of PANI(PEOPA)$_R$ complexes with different binding fractions. The correlation function of the complex with $R = 0.5$ displays a comparatively slow damping than that of the other compositions, indicating the most coherent lamellar stacking. This observation is in accord with the SAXS profile in Figure 3 where the complex with $R = 0.5$ exhibits a relatively sharper peak than the other compositions. A more planar conformation of PANI chains at the stoichiometric doping ratio as inferred from UV−vis results may be the reason for better lamellar organization in this composition.

The interlamellar distance and the individual layer thicknesses obtained from the correlation function analysis are plotted as a function of binding fraction in Figure 6. Both the interlamellar distance and d_{PEO} are seen to increase with increasing R, whereas d_{PANI} remains approximately constant at ca. 1.70 nm. The PEO layer thickness varies in the range 3.64−4.10 nm. The unperturbed dimension of PEO chain with a molecular weight of 550 is ∼1.97 nm,[37] whereas its extended chain length would be 3.48 nm.[38] On the basis of the observed d_{PEO}, it can be assumed that each nonionic layer contains a bilayer of PEO chains with a limited interdigitation, as schematically illustrated in Figure 4. Figure 7 presents a probable schematic illustration for explaining the composition variation of d_{PEO}. As the binding fraction increases, the number density of PEO chains grafted at PANI backbone (and hence the lamellar interface) increases. It must be noted here that though the stoichiometric binding fraction is $R = 0.5$, the uncomplexed PEO chains at higher binding

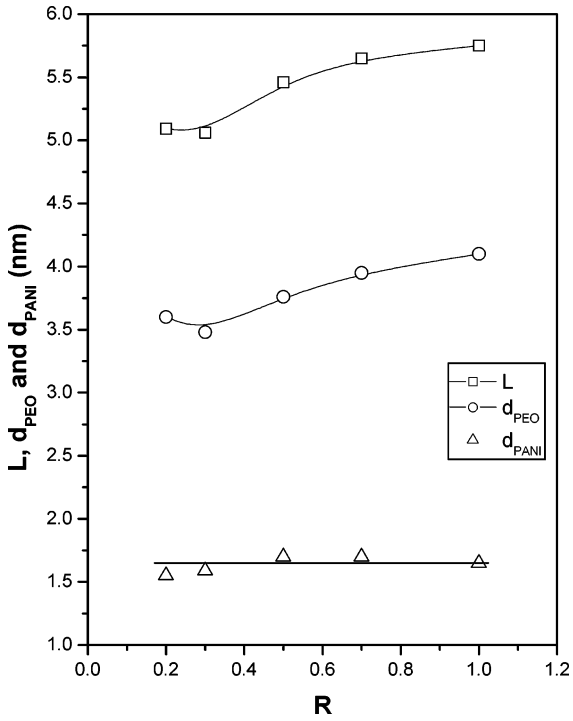

Figure 6. Composition variations of interlamellar distance (L), PANI layer thickness (d_{PANI}), and PEO layer thickness (d_{PEO}) of PANI(PEOPA)$_R$ complexes.

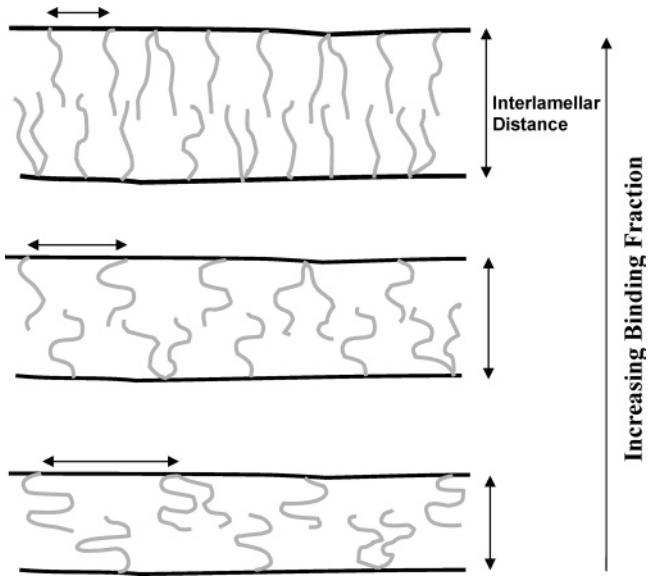

Figure 7. Schematic illustration describing the effect of binding fraction on the thickness of PEO layer. An increase in binding fraction reduces the interfacial area per PEO side chain which then drives the PEO chains to stretch in a direction normal to the interface in order to maintain the normal liquid density.

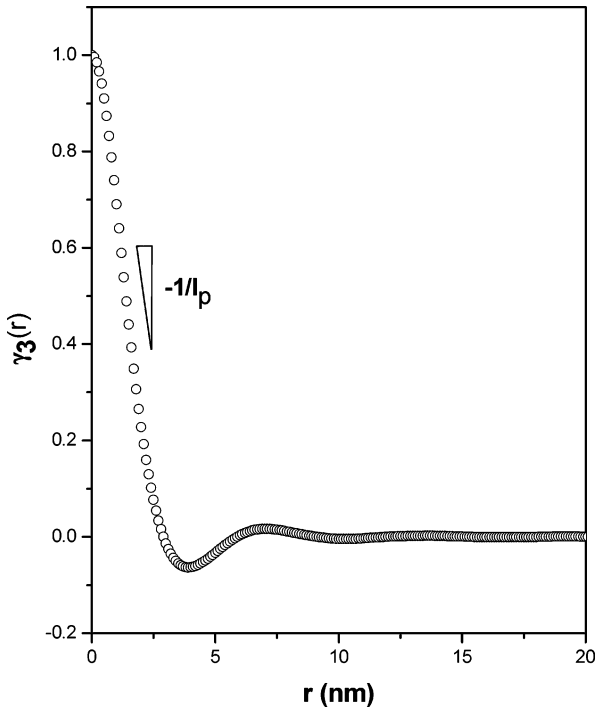

Figure 8. A representative three-dimensional correlation function calculated from the SAXS profile of PANI(PEOPA)$_R$ complex with $R = 0.5$. The Porod length (l_p) is determined from the initial linear region of the plot according to eq 4.

fraction may still be bonded to PANI chains at their aminic sites through hydrogen bonding via their hydroxyl groups. The increased density of PEO chains at the lamellar interface reduces the interfacial area per PEO chain, and hence the chains have to stretch normal to the interface to attain the normal liquid density. Hence, the PEO layer thickness swells accordingly leading to an increase of the interlamellar distance.

Since the SAXS profiles obey Porod's law at high q, a three-dimensional averaged length between the phase boundary known as the average chord length (l_p) of a two-phase system can be calculated using the three-dimensional correlation function defined as

$$\gamma_3(r) = \frac{\int_0^\infty I(q) q^2 \sin(qr)/qr \, \mathrm{d}q}{\int_0^\infty I(q) q^2 \, \mathrm{d}q} \tag{3}$$

Porod's law at large q prescribes $\gamma_3(r)$ to adopt the following form at small radial distance:

$$\gamma_3(r) = 1 - \frac{1}{l_p} \tag{4}$$

According to eq 4, l_p can be determined from the slope of $\gamma_3(r)$ plot at small r, as demonstrated in Figure 8 for the complex with $R = 0.5$. The values of l_p so estimated are tabulated in Table 2. l_p is found to lie in the range of 1.94−2.22 nm and exhibits the same composition dependence as the interlamellar distance or d_{PEO}. In the lamellar two-phase system, l_p is related to the average thicknesses of the constituting layers by $l_p = 2\phi_{PANI}d_{PANI} = 2\phi_{PEO}d_{PEO}$, where ϕ_i is the volume fraction of layer i in the lamellar stack.[39] Consequently, l_p for a lamellar system must lie in the range of $0 \le l_p \le (d_{PANI} + d_{PEO})/2 = L/2$. l_ps are found to situate within this range for all

Table 2. Structural Parameters Deduced from the SAXS Data Analysis

binding fraction (R)	l_p (nm)[a]	$S/S_0 = 2d_{PANI}d_{PEO}/Ll_p$[b]
1.0	2.22	1.06
0.7	2.21	1.08
0.5	2.11	1.11
0.3	2.00	1.03
0.2	1.94	1.07

[a] Determined from the three-dimensional correlation function. [b] L, d_{PANI}, and d_{PEO} were determined from a one-dimensional correlation function.

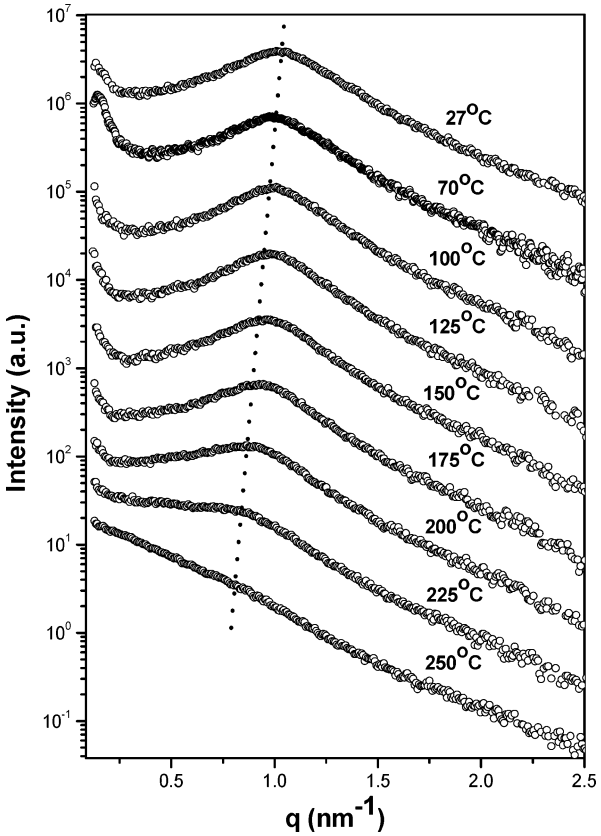

Figure 9. Temperature-dependent SAXS profiles of PANI(PEOPA)$_R$ complex with $R = 0.5$ collected in a heating cycle. The scattering peak shifts to lower q and broadens with the increase of temperature. An order−disorder transition was observed near 225 °C, where a monotonically decayed profile typical of disordered system is identified.

compositions under study, which further supports the formation of lamellar mesophase in the complexes.

In addition to the lamellar thicknesses, the curvature of the interface between ionic and nonionic layers is an important characteristic of the morphology. For a planar interface the total interfacial area per unit volume is given by $S_0/V = 2/L$. If the interface is not planar, the total S/V would be larger than $2/L$.[40,41] A measure of the planarity of the interface is hence given by the ratio

$$\frac{S}{S_0} = \frac{2d_{PANI}d_{PEO}}{Ll_p} \tag{5}$$

The values of S/S_0 obtained for different binding fractions of the complexes are also shown in Table 2. The proximity of the calculated ratios to 1.0 irrespective of composition attests that the lamellar interfaces in the complexes are planar.

The effect of temperature on the microphase-separated structure is examined by the temperature-

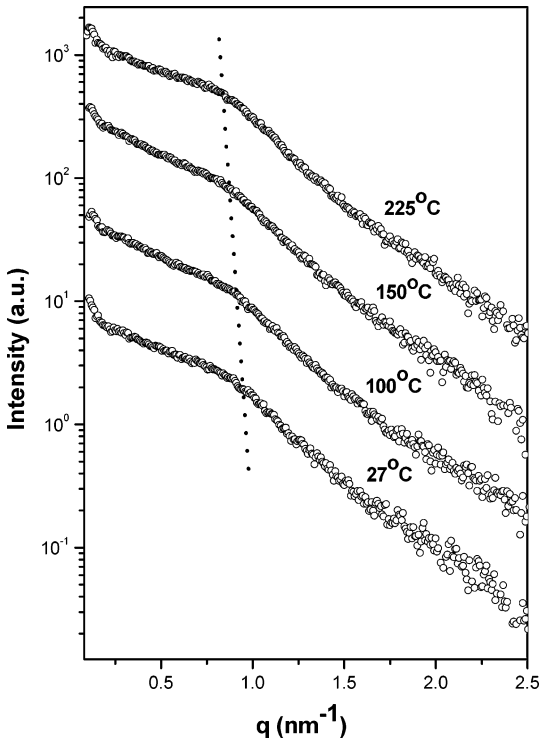

Figure 10. Temperature-dependent SAXS profiles of PANI-(PEOPA)$_R$ complex with $R = 0.5$ collected in a cooling cycle from 225 °C.

dependent SAXS experiment. Figure 9 displays a series of SAXS profiles of the PANI(PEOPA)$_R$ complex with $R = 0.5$ as recorded in a heating cycle. The SAXS peak shifts to lower q, signaling an increase of L and broadens with increasing temperature. The swelling of interlamellar distance is attributed to the thermal expansion effect, where the rigid PEO-bound PANI restricts the lateral expansion of the PEO layers such that the thermal expansion occurs predominantly along the thickness direction. The scattering peak is replaced by a monotonically decayed profile corresponding to a disordered morphology at 250 °C. It has been shown for protonated PANI salts that a slow deprotonation started above 100 °C. The rate of deprotonation increased after 180 °C and completed only above 200 °C.[42] Hence, the increase of the SAXS peak breadth may be related to the occurrence of decomplexation at elevated temperatures. Below 200 °C the deprotonation process is slow, and its extent increases with increasing temperature. At 250 °C not only deprotonation completes but also degradation of PEOPA starts which leads to complete disappearance of the SAXS peak. Thermogravimetric analysis of PANI(PEOPA)$_R$ complexes also shows a significant weight loss starting at ca. 240 °C.

To ascertain whether the deprotonation/reprotonation process is reversible, a SAXS cooling experiment was conducted after the sample was heated to 225 °C. This temperature was selected to avoid the interference from thermal degradation. Figure 10 shows the SAXS profiles of the complex with $R = 0.5$ collected in situ during the cooling cycle. No appreciable change in scattering pattern is observed, indicating a negligible reprotonation, if any, of PANI chains upon cooling. It has been reported that reprotonation of PANI chains on cooling is very slow and may take weeks to observe any significant level of reprotonation.[42,43] One of the explanations may be that the protons generated on deprotonation may combine with their phosphate counterions to regenerate

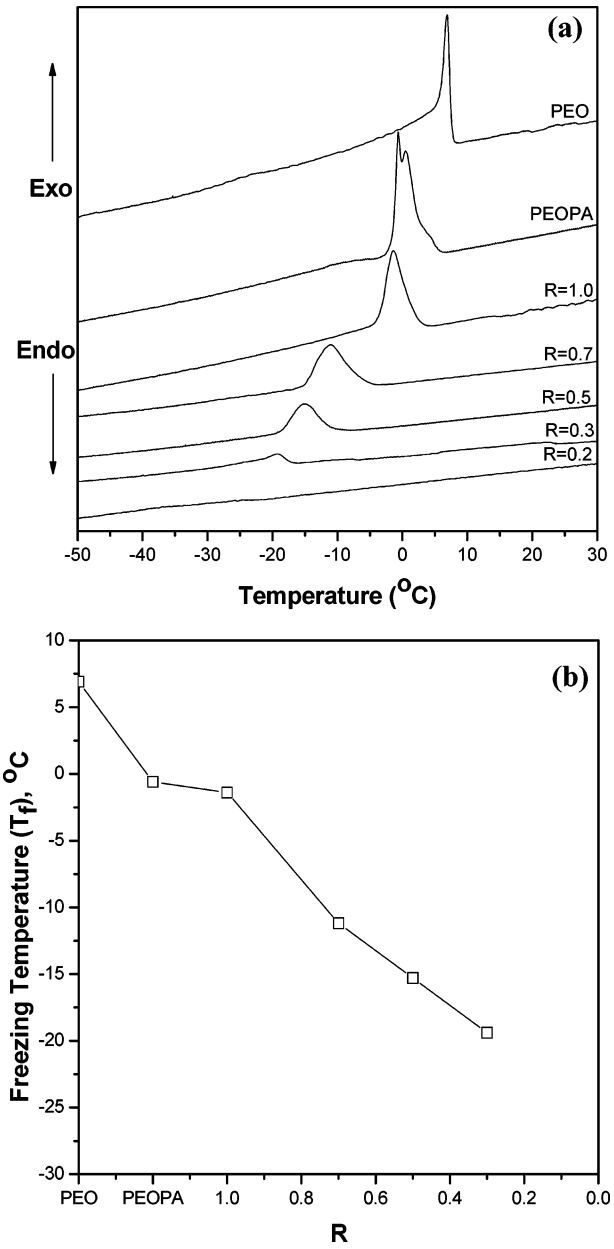

Figure 11. (a) Representative crystallization exotherms recorded at a cooling rate of 1 °C/min for PANI(PEOPA)$_R$ complexes. (b) Variation of freezing temperature (i.e., the peak temperature of the exotherm) as a function of binding fraction.

the neat PEOPA and undoped PANI. Since the system is now in bulk state rather than in a solvent medium, reprotonation will be very difficult because of the sluggish diffusion of individual polymeric species.

Crystallization Behavior of PEO Side Chains in the Lamellar Microdomains. The side-chain crystallization in *covalently bonded* comblike polymers has been extensively investigated; however, not much attention has been given to the same aspect in supramolecular comb polymer systems. Recently, Luyten et al. have reported the crystallization behavior of alkyl side chains in hydrogen-bonded supramolecular comb polymers based on their melting behavior.[44] Their results were very similar to those observed for the covalently bonded comb polymers.[4]

A nonisothermal crystallization study is carried out here to examine the crystallization kinetics of the PEO side chains in PANI(PEOPA)$_R$ complexes. Figure 11a

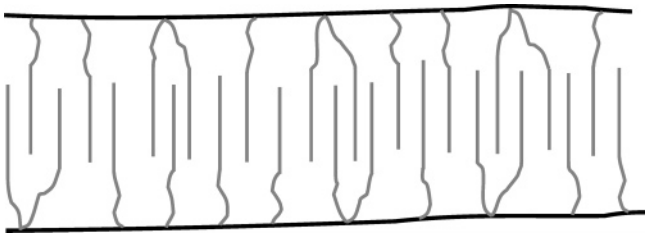

Figure 12. Schematic illustration of the proposed crystalline structure of PANI(PEOPA)$_R$ complexes. PEO chains are assumed to crystallize in extended chain conformation due to very low molecular weight. A noncrystalline transition layer situates between the crystalline phase and the lamellar interface for dissipating the mismatch in PEO segmental densities in these two regions.

shows the crystallization exotherms of PEO, PEOPA, and the complexes recorded by cooling at 1 °C/min. Well-defined crystallization exotherms can be observed over the composition range studied. It is noted that neat PEO and its corresponding phosphate ester, i.e., PEOPA, follow different crystallization behavior. Neat PEO shows a single crystallization peak whereas PEOPA displays at least three peaks. The crystallization kinetics of PEOPA is also slower as manifested by the lower freezing temperature (i.e., the peak temperature of the exotherm). The multiple crystallization exotherms can be related to the fact that PEOPA is indeed a mixture of two different structures (cf. Scheme 1); one is a linear chain with one end terminated by a bihydroxylphosphoric acid, and the other is a two-arm PEO connected by a monohydroxylphosphoric acid which in one way acts as a defect between the PEO chains. The single- and two-arm chains may crystallize separately, leading to multiple crystallization exotherms, and the additional demixing step involved in such a segregated crystallization slows down the crystallization kinetics in PEOPA.

A single crystallization exotherm is identified for the complexes irrespective of binding fraction and cooling rates, showing that the segregation between single- and two-arm PEO chains during crystallization is effectively suppressed due to random binding of these two kinds of chains to the PANI backbone that is too rigid to allow the conformational rearrangement for accommodating the phase segregation. In this case, the single- and two-arm chains cocrystallize with a cooperative crystallization mechanism. Figure 12 shows the proposed crystalline layer structure of PANI(PEOPA)$_R$ complexes, in which PEO chains are assumed to crystallize in the extended-chain conformation due to low molecular weight. It has been found that the side chains of comb polymers crystallized in either an interdigitating or an end-to-end packing.[4,45] One of the factors which influences the type of packing is the rigidity of main chain.[46] A flexible backbone can adjust very well to close packing of the side chains and hence favors end-to-end type of packing. Enhanced rigidity of the backbone results in severe hindrance to close packing of the side chains, and hence crystallization is achieved by packing the chains in the interdigitating form. Considering the rigid nature of the PANI backbone in the present complex, an interdigitating packing of PEO chains in the crystalline layer should be the most probable.

Figure 11b plots the freezing temperatures (T_f) of the complexes as a function of binding fraction. The complexes exhibit slower crystallization than neat PEOPA and neat PEO; therefore, tethering a chain end to PANI

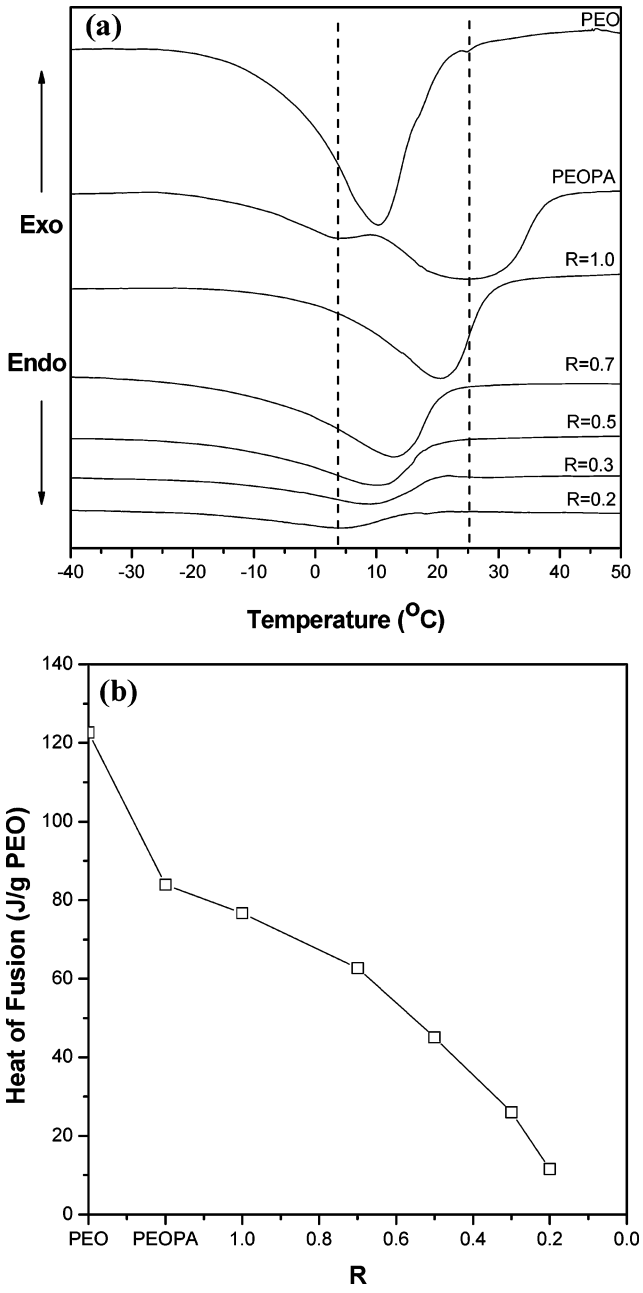

Figure 13. (a) Representative melting endotherms recorded at a heating rate of 10 °C/min of the complexes having been cooled at 1 °C/min to −60 °C. (b) Variation of heat of fusion (normalized by the PEO weight fraction) with the binding fraction of PANI(PEOPA)$_R$ complexes.

backbone reduces the crystallization kinetics in that the conformational rigidity of PANI coupled with the ionic bonding strongly restricts the diffusion of PEO chains involved in crystal growth. For the complexes, T_f is found to drop progressively with decreasing R. The slower crystallization rate at smaller R may be attributed to the greater separation distance between the junction points of PEO chains along the PANI backbone.

Figure 13a shows the melting endotherms of the complexes having been cooled at 1 °C/min to −60 °C. Neat PEOPA displays two broad peaks in the melting region, which may be associated with the crystalline phases formed by single- and two-arm PEO chains. A single melting endotherm situating between the two melting peaks of PEOPA is identified for the complexes, which further demonstrates cocrystallization of the PEO

chains. Decreasing binding fraction tends to reduce the melting temperature (T_m). Luyten et al. have observed a similar T_m depression for the hydrogen-bonded complexes of poly(4-vinylpyridine) (P4VP) and pentadecylphenol (PDP).[44] Their explanation for the observation was based on the entropy loss of P4VP main chains as it formed complex with PDP. Since more P4VP segments are involved per same amount of PDP molecules for smaller binding fraction, the entropy loss is larger. Apart from this explanation, the depression of T_m in the present PANI(PEOPA)$_R$ complexes may be related to the mismatch between the segmental density of PEO (in terms of number of PEO segments per unit area) near the lamellar interface (prescribed by the binding density with the PANI backbone) and that in the crystal. In this case, a noncrystalline transition layer, which becomes thicker at lower R due to the greater separation distance between the junction points at PANI backbone, is required to dissipate such a density mismatch as one proceeds from the crystalline phase to the lamellar interface along the lamellar normal (cf. Figure 12). The presence of this transition layer reduces both the crystallinity and the crystal thickness of PEO; therefore, T_m is depressed accordingly.

Figure 13b shows the variation of the degree of crystallinity represented by the heat of fusion (normalized by the PEO weight fraction in the sample) with R. The crystallinity of neat PEOPA is less than that of neat PEO because the presence of bulky end groups in the former results in higher defects in its crystal structure. The crystallinity in the complex also decreases progressively with decreasing R. This is in accord with the foregoing suggestion that the thickness of the transition layer (whose presence reduces the crystallinity) increases with decreasing binding fraction. Similar results have been reported by Luyten et al. in the case of P4VP(PDP) complexes.[44] Similarly, for covalently bonded comb polymers, Inomata et al. had noticed a decrease of the crystallization enthalpy with decrease in side chain density.[47,48]

Conclusions

The self-assembled structures and crystallization behavior of PANI(PEOPA)$_R$ hairy rod complexes in the bulk state have been investigated. The complexes exhibited a microphase-separated lamellar structure consisting of ionic and nonionic layers. The ionic layer composed of PANI backbones and the ionic headgroups of PEOPA, whereas the nonionic layer consisted of PEO side chains. The PEO layer thickness increased with increasing binding fraction because of higher chain stretching as the separation distance between the junction points at the PANI backbone increased. From the layer thicknesses and Porod length estimated using three-dimensional correlation function, the lamellar interface was found to be almost planar. The SAXS heating experiment revealed an order−disorder transition near 225 °C due to deprotonation in the complex. The reprotonation upon subsequent cooling was however negligible. Complexation with PANI exerted a strong influence on the crystallization behavior of PEO. The segregation between single- and two-arm PEO chains during crystallization found in neat PEOPA was effectively suppressed in the complexes. The crystallization kinetics, melting temperature, and degree of crystallinity of PEO were found to drop with decreasing binding fraction. The depressions of melting temperature and crystallinity were related to the presence of a noncrystalline transition layer, which became thicker at lower R, situating between the crystalline phase and the lamellar interface for dissipating the mismatch in PEO segmental densities in these two regions.

Acknowledgment. We gratefully acknowledge financial support from the Ministry of Education and the National Science Council under Contract Nos. 91E-FA04-2-4A and NSC92-2216-E-110-009, respectively.

References and Notes

(1) Bates, F. S.; Fredrickson, G. H. *Annu. Rev. Phys. Chem.* **1990**, *41*, 525.
(2) Hamley, I. W. *The Physics of Block Copolymers*; Oxford University Press: Oxford, 1998.
(3) Fischer, H.; Poser, S. *Acta Polym.* **1996**, *47*, 413.
(4) Plate', N. A.; Shibaev, V. P. *Comb-Shaped Polymers and Liquid Crystals*; Plenum Press: New York, 1987.
(5) Ballauff, M. *Angew. Chem., Int. Ed. Engl.* **1989**, *28*, 253.
(6) Wegner, G. *Thin Solid Films* **1992**, *216*, 105.
(7) Lauter, U.; Meyer, W. H.; Wegner, G. *Macromolecules* **1997**, *30*, 2092.
(8) Wegner, G. *Macromol. Chem. Phys.* **2003**, *204*, 347.
(9) Antonietti, M.; Conrad, J.; Thünemann, A. *Macromolecules* **1994**, *27*, 6007.
(10) Ikkala, O.; Ruokolainen, J.; ten Brinke, G.; Torkkeli, M.; Serimaa, R. *Macromolecules* **1995**, *28*, 7088.
(11) Ruokolainen, J.; ten Brinke, G.; Ikkala, O.; Torkkeli, M.; Serimaa, R. *Macromolecules* **1996**, *29*, 3409.
(12) Antonietti, M.; Burger, C.; Thünemann, A. *Trends Polym. Sci.* **1997**, *5*, 262.
(13) ten Brinke, G.; Ikkala, O. *Trends Polym. Sci.* **1997**, *5*, 213.
(14) Zheng, W.-Y.; Wang, R.-H.; Levon, K.; Rong, Z. Y.; Taka, T.; Pan, W. *Makromol. Chem. Phys.* **1995**, *196*, 2443.
(15) Ikkala, O.; Knaapila, M.; Ruokolainen, J.; Torkkeli, M.; Serimaa, R.; Jokela, K.; Horsburgh, L.; Monkman, A. P.; ten Brinke, G. *Adv. Mater.* **1999**, *11*, 1206.
(16) Chen, H. L.; Hsiao, M. S. *Macromolecules* **1999**, *32*, 2967.
(17) Ruokolainen, J.; Eerikainen, H.; Torkkeli, M.; Serimaa, R.; Jussila, M.; Ikkala, O. *Macromolecules* **2000**, *33*, 9272.
(18) Ruokolainen, J.; Lahtinen, M.; Torkkeli, M.; Serimaa, R.; Valkonen, J.; Rissanen, K.; Ikkala, O. *Macromolecules* **2001**, *34*, 7789.
(19) Chen, H. L.; Ko, C. C.; Lin, T. L. *Langmuir* **2002**, *18*, 5619.
(20) Stepanyan, R.; Subbotin, A.; Knaapila, M.; Ikkala, O.; ten Brinke, G. *Macromolecules* **2003**, *36*, 3758.
(21) Knaapila, M.; Stepanyan, R.; Horsburgh, L. E.; Monkman, A. P.; Serimaa, R.; Ikkala, O.; Subbotin, A.; Torkkeli, M.; ten Brinke, G. *J. Phys. Chem. B* **2003**, *107*, 14199.
(22) Geng, Y. H.; Sun, Z. C.; Li, J.; Jing, X. B.; Wang, X. H.; Wang, F. S. *Polymer* **1999**, *40*, 5723.
(23) Wang, Y.; Wang, X.; Li, J.; Zhang, H.; Mo, Z.; Jing, X.; Wang, F. *J. Polym. Sci., Polym. Phys. Ed.* **2002**, *40*, 605.
(24) Chen, S. A.; Lee, H. T. *Macromolecules* **1993**, *26*, 3254.
(25) Porod, G. *Kolloid-Z.* **1951**, *124*, 83.
(26) Porod, G. *Kolloid-Z.* **1952**, *125*, 51.
(27) Ruland, W. J. *J. Appl. Crystallogr.* **1971**, *4*, 70.
(28) Lu, F. L.; Wudl, F.; Nowak, M.; Heeger, A. J. *J. Am. Chem. Soc.* **1986**, *108*, 8311.
(29) Stafstorm, S.; Bredas, J. L.; Epstein, A. J.; Woo, H. S.; Tanner, D. B.; Huang, W. S.; MacDiarmid, A. G. *Phys. Rev. Lett.* **1987**, *59*, 1464.
(30) Hopkins, A. R.; Rasmussen, P. G.; Basheer, R. A. *Macromolecules* **1996**, *29*, 7838.
(31) Ornstein, L. S.; Zernike, F. *Proc. Acad. Sci. Amsterdam* **1914**, *17*, 793.
(32) Perahia, D.; Vacca, G.; Patel, S. S.; Dai, H. J.; Balsara, N. P. *Macromolecules* **1994**, *27*, 7645.
(33) Strobl, G. R.; Schneider, M. *J. Polym. Sci., Polym. Phys. Ed.* **1980**, *18*, 1343.
(34) Debye, P.; Bueche, A. M. *J. Appl. Phys.* **1949**, *20*, 518.
(35) Debye, P.; Anderson Jr., H. R.; Brumberger, H. *J. Appl. Phys.* **1957**, *28*, 679.
(36) Vonk, C. G. *J. Appl. Crystallogr.* **1978**, *11*, 541.
(37) *37. Polymer Handbook*, 3rd ed.; Brandrup, J., Immergut, E. H., Eds.; Wiley: New York, 1989.
(38) Kovacs. A. J.: Straupe, C. *Faraday Discuss. Chem. Soc.* **1979**, *68*, 225.

(39) Ruland, W. *Colloid Polym. Sci.* **1977**, *255*, 417.
(40) Thünemann, A. F.; Lochhaas, K. H. *Langmuir* **1998**, *14*, 6220.
(41) Thünemann, A. F.; Schnöller, U.; Nuyken, O.; Voit, B. *Macromolecules* **1999**, *32*, 7414.
(42) Yang, C. Y.; Reghu, M.; Heeger, A. J.; Cao, Y. *Synth. Met.* **1996**, *79*, 27.
(43) Chen, S. A.; Lee, H. T. *Macromolecules* **1995**, *28*, 8, 2858.
(44) Luyten, M. C.; Alberda van Ekenstein, G. O. R.; ten Brinke, G.; Ruokolainen, J.; Ikkala, O.; Torkkeli, M.; Serimaa, R. *Macromolecules* **1999**, *32*, 4404.
(45) Hsieh, H. W. S.; Post, B.; Morawetz, H. *J. Polym. Sci., Polym Phys. Ed.* **1976**, *14*, 1241.
(46) Kricheldorf, H. R.; Domschke, A. *Macromolecules* **1996**, *29*, 1337.
(47) Inomata, K.; Sakamaki, Y.; Nose, T.; Sasaki, S. *Polym. J.* **1996**, *28*, 986.
(48) Inomata, K.; Sakamaki, Y.; Nose, T.; Sasaki, S. *Polym. J.* **1996**, *28*, 992.

MA048384R